applied sciences

MDPI

Article

NO_x Reduction Pathways during LNT Operation over Ceria Containing Catalysts: Effect of Copper Presence and Barium Content

Juan Carlos Martínez-Munuera [1], Javier A. Giménez-Mañogil [1], Roberto Matarrese [2], Lidia Castoldi [2,*] and Avelina García-García [1,*]

[1] MCMA Group, Department of Inorganic Chemistry and Institute of Materials, University of Alicante, Carretera San Vicente del Raspeig s/n, San Vicente del Raspeig, 03690 Alicante, Spain; jc.martinez@ua.es (J.C.M.-M.); javierantonio.gimenez@ua.es (J.A.G.-M.)

[2] Laboratory of Catalysis and Catalytic Processes, Dipartimento di Energia, Politecnico di Milano, Via La Masa 34, 20156 Milano, Italy; roberto.matarrese@polimi.it

* Correspondence: lidia.castoldi@polimi.it (L.C.); a.garcia@ua.es (A.G.-G.); Tel.: +39-02-2399-3255 (L.C.); +34-965-909-419 (A.G.-G.)

Abstract: Ceria-based catalysts, with Cu in substitution of noble metals, were studied in a vertical microreactor system under isothermal conditions, where NO_x was previously stored, followed by the reduction step conducted under H_2. The possible remaining ad-NO_x species after the reduction stage, were investigated by Temperature Programmed Desorption in He. In situ DRIFTS was used as a complementary technique for the analysis of the surface species formation/transformation on the catalysts' surface. Catalysts containing both Ba and Cu were found to be selective in the NO_x reduction, producing N_2 and minor amounts of NH_3 during the reduction step, as well as NO. The different ceria-based formulations (containing copper and/or barium) were prepared and tested at two different temperatures in the NO_x reduction (NSR) processes. Their catalytic activities were analyzed in terms of their compositions and have been useful in the elucidation of the possible origin and relevant pathways for NO_x reduction product formation, which seems to involve the oxygen vacancies of the ceria-based materials (whose generation seems to be promoted by copper) during the rich step. The scope of this work involves an interdisciplinary study of the impact that catalysts' formulations (noble metal-free) have on their LNT performance under simulated conditions, thus covering aspects of Materials Science and Chemical Engineering in a highly applied context, related to the development of control strategies for hybrid powertrains and/or the reduction of the impact of cold-start emissions.

Keywords: exhaust aftertreatment systems; LNT (lean NO_x trap); ceria–zirconia; copper species; barium; NO_x reduction; oxygen vacancies.

Citation: Martínez-Munuera, J.C.; Giménez-Mañogil, J.; Matarrese, R.; Castoldi, L.; García-García, A. NO_x Reduction Pathways during LNT Operation over Ceria Containing Catalysts: Effect of Copper Presence and Barium Content. *Appl. Sci.* **2021**, *11*, 5700. https://doi.org/10.3390/app11125700

Academic Editors: Pedro Piqueras and Joaquin de la Morena

Received: 13 May 2021
Accepted: 16 June 2021
Published: 19 June 2021

1. Introduction

Europe has proposed ambitious reductions in CO_2 limits for both light- and heavy-duty sectors, and discussions have already started on the continent regarding the next level of regulations, beyond Euro 6 [1]. Original Equipment Manufacturers (OEMs) are testing approaches for meeting these tough targets, both for reducing CO_2 and tailpipe NO_x through improved engine and after-treatment technologies [2].

NO_x emissions from in-use diesel vehicles have come under intense scrutiny, and while meeting current and upcoming regulations is a significant challenge, several studies have been carried out to demonstrate that diesels can be very clean under a wide range of operating conditions [3].

Various recent studies support that engine improvements coupled with advanced after-treatment systems enable vehicles to meet post-Euro 6 NO_x limits under challenging real-world driving conditions. It is clear that only the use of combined after-treatment technologies would permit the achievement of these stringent limits. Some authors report very low NO_x emissions using a combination of LNT (Lean NO_x Trap), SCR, and an ammonia slip catalyst under demanding urban driving conditions [4]; others propose the use of a type of non-hybrid 2.0 L D-segment vehicle in combination with LNT, catalyzed DPF, and down-stream SCR [5]. Very recent studies demonstrate that LNT and SCR coated filters offer further cold start emission reduction, and that the innovative diesel mild hybrids can offer synergistic gains for lower NO_x as well as CO_2 improvements [2].

Taking these premises into account, LNTs are still an interesting technology in the framework of a combined diesel or lean-burn engine strategy for efficient NO_x removal; lean combustion would need a complete rework of exhaust aftertreatment systems on gasoline engines, which traditional three-way catalysts (TWC) could not operate. Under these multiple contexts, LNT catalysts should be able to store NO_x in a temperature window between 150 °C and 350 °C under lean conditions, and subsequently reduce them under rich conditions; during this step, together with N_2, some NH_3 can be formed that could assist the downstream SCR device. However, several catalyst formulations, mainly based on zeolite doped with noble metals like Pd, could permit the storage of NO_x at low temperatures, subsequently releasing them at a higher temperature for the proper operation of the downstream SCR element [2]. All these actions can yield a lot of benefits and create a complex interplay in the design of new generation after-treatment strategies. An investigation of the influence of the various components forming these catalysts deserves special attention.

LNT catalysts operate under cyclic conditions. In the first step, under lean conditions (that is, in excess of oxygen), NO_x is stored onto the catalyst's surface in the form of nitrites and/or nitrates depending on the storage temperature, while in the second step, the stored NO_x is reduced under rich conditions, with N_2 as a main product [6–16]. Nevertheless, some other products might be formed, such as NO, NO_2, NH_3, or N_2O, because of an inefficient reduction or thermal decomposition. Typically, LNT catalysts are constituted of noble metals (Pt, Pd, Rh), which efficiently oxidize NO to NO_2 under O_2 and favor the generation of reduced N-products during the rich phase; they are also comprised of alkaline or alkaline earth metal oxides (Ba, K) as the storage component [10,13,15,17–19]. The catalytic NO oxidation to NO_2 is a critical point due to the relevance of the NO_2 presence in different depollution technologies [20–23]; indeed, not only can NO_2 be effectively retained onto catalytic NSR storage components, thus increasing the NO_x removal capacity of these systems, but it can also be very active in soot oxidation, being more oxidant than O_2. Thus, NO_2-assisted soot combustion processes are interesting for the proper regeneration of diesel particulate filters (DPF), as well as in diesel particulate-NO_x reduction systems (DPNR) for the simultaneous removal of both contaminants [24–27].

Ceria is a common component in several traditional automotive catalytic systems, such as three-way catalysts (TWCs) [6,7], due to its unique properties. First of all, its oxygen storage capacity (OSC), which allows for the regulation of oxygen partial pressure under atmosphere changes. Cerium-based oxides, combined with Zr or Pr, are frequently used as redox catalysts in a number of applications [28–31]; cerium oxide is also present in significant amounts in LNT catalyst formulations [32] to increase thermal stability and add OSC functionality [11]. Some authors have reported improved NO_x storage capacity (particularly at moderate temperatures, 200–400 °C) [33] when including ceria as an ingredient in the formulations of these catalysts linked to a high basic character of ceria and to a relevant surface/bulk oxygen mobility. Additionally, the resultant ad-NO_x species are quite reactive under H_2 or either CO [34].

However, LNT catalysts suffer of some drawbacks, one of them being the use of high-cost noble metals in LNT formulations. Therefore, efforts have been made in order to sub-

stitute Pt with other metals; Cu has been proposed as a possible candidate [35–38]. In addition, interesting properties have been found upon the combination of Cu and ceria; for example, these catalysts present a highly promoted NO oxidation to NO_2 (at low–mild temperatures) and a very high reducibility at low temperatures as well. These improved characteristics have been attributed to a synergistic effect between CuO_x sites and ceria's surface, which is due to their interfacial interactions that promote redox behavior [39–43]. The higher capacity of NO and/or NO_2 oxidation has also been exploited by our group, studying copper/ceria–zirconia catalysts in soot combustion processes (under NO + O_2 and under O_2 atmospheres) [44–47]. Nevertheless, a comprehensive study of the possibilities towards the NO_x reduction of these catalysts is still lacking. Therefore, the scope of this work involves an interdisciplinary study of the impact that catalysts' formulations (noble metal-free) have on their LNT performance under simulated conditions, thus covering aspects of Materials Science and Chemical Engineering in a highly applied context, related to the development of control strategies for hybrid powertrains and/or the reduction of the impact of cold-start emissions, thus connecting with the aims and scope of the Journal of Applied Sciences and with those of this Special Issue.

In a previous work [48], we prepared and fully characterized new LNT catalysts based on Cu/(Ba)/ceria–zirconia components. These catalytic systems were tested in NO_x adsorption at different temperatures in the range of 150–350 °C. The catalytic results reported that Cu enhances the NO oxidation activity, which is lowered by the presence of Ba. On the other hand, Ba benefits the NO_x storage capacity, and consequently, the sample containing both Cu and Ba, with the formulation Cu(2% *w*/*w*)/Ba(6% *w*/*w*)/$Ce_{0.8}Zr_{0.2}O_2$ showing the highest NO_x storage capacity among the investigated samples.

In this study, we complete the analysis of these systems considering only the reduction step, an analysis of the catalysts' formulations (support alone, presence of Cu and/or Ba, loading of Ba), and the effect of the reaction temperature. Finally, some insights into the processes governing NSR operation by this type of noble metal-free ceria-based catalysts are elucidated, focusing on low temperatures and predominant routes of NO_x reduction with these novel formulations. These elucidations will provide new useful knowledge for the design of subsequent combinations of these systems with other after-treatment technologies.

2. Materials and Methods

2.1. Catalyst Preparation

The synthesis of ceria–zirconia (CZ), with $Ce_{0.8}Zr_{0.2}O_2$ as the specific formulation, is well-described elsewhere [44,49,50]. In summary, ceria–zirconia was prepared by co-precipitation of the corresponding precursor salts, $(NH_4)_2Ce(NO_3)_6$ and $ZrO(NO_3)_2{\cdot}x\ H_2O$, in alkali media. The solids obtained were dried and calcined in air at 500 °C for 1 h.

Cu2/CZ samples (Cu loading 2% *w*/*w*) was prepared by incorporating the copper precursor to CZ by the incipient wetness impregnation method; this Cu loading was selected according to our previous study [44]. As reported elsewhere [44], the catalyst was prepared by incipient wetness impregnation, using $Cu(NO_3)_2{\cdot}3H_2O$ as precursor; then, the system was dried and calcined in air at 500 °C for 1 h.

Finally, the barium precursor was incorporated to CZ and Cu2/CZ by wetness impregnation. The corresponding procedure, described in detail elsewhere [48], involved the dissolution of proper amounts of barium acetate in the minimum amount of water required in order to impregnate CZ and Cu2/CZ. The solids were dried and calcined in air at 500 °C for 1 h. Considering the nominal amounts of Ba wt % achieved in the solids, they were named as Ba6/CZ, Ba6/Cu2CZ, and Ba11/Cu2CZ, respectively (see the corresponding theoretical and experimental quantification by means of X-ray fluorescence technique elsewhere [48]).

2.2. Characterization Techniques

All the samples were characterized in depth by means of XRF, N_2 adsorption-desorption isotherms at −196 °C, XRD, Raman spectroscopy, H_2-TPR, XPS, and in situ DRIFTS; details of the characterization were previously described [48] and briefly reported in this article for completeness. Details of the cited experimental techniques are compiled under the Supplementary Information. The XRD spectra showed that the Ba phase was present as carbonates in the fresh Ba-containing catalysts. Barium incorporation into the catalyst formulation led to a certain pore blocking and a decrease of the surface area, along with a very minor decrease of catalyst reducibility, as revealed by H_2-TPR. At variance, Cu significantly increased catalyst reducibility. From XPS, it was confirmed that both Cu and Ba were enriched on the catalyst's surface, i.e., they might not be significantly hidden or incorporated into the CZ lattice.

2.3. Catalytic Activity Experiments

The catalytic tests were carried out in a tubular quartz reactor, coupled with different analyzers in parallel: a mass spectrometer, a micro-gas chromatograph, and a UV-NO_x analyzer. A total of 60 mg of catalyst was used for each experiment and the total inlet gas flow was kept at 100 mL/min during the experiment (GHSV = 100,000 h^{-1}).

The NO_x adsorption/reduction cycles were performed at a constant temperature in the range 150–350 °C (with the exception of Ba6/CZ that was only investigated under 250–350 °C). In a typical experiment, the catalyst was pre-treated in inert atmosphere at 500 °C for 30 min; then, it was cooled down to the adsorption/reduction temperature. The adsorption phase was carried out by feeding to the reactor 1000 ppm of NO + 3% *v*/*v* of O_2 in He (as balance), up to catalyst saturation. After ca. 1 h, NO and O_2 concentrations were decreased stepwise to zero, followed by He purge at the same temperature. The subsequent reduction step was performed by feeding to the reactor 2000 ppm H_2 in He (as balance) during a variable time, but around 1 h in most of the cases. The reason for this variability is the different rates of decay of MS signals and/or the different reactivities of the catalysts at the two temperatures of interest. Nevertheless, the time was kept until all the N-reduction product emissions decayed in all the cases. Finally, to ensure a complete release/decomposition of the previously adsorbed NO_x species (in case they were not reduced during the reduction step), Temperature Programmed Desorption (TPD) was performed by increasing the temperature progressively up to 500 °C under He (10 °C/min).

An additional experiment consisting of consecutive pulses of NO + O_2 (for 20 min each) and subsequent pulses of H_2 (for 15 min each) was performed for the Ba6/Cu2CZ sample at a constant temperature of 300 °C and using the same gas concentrations. After finishing these cycles, a TPD was carried out, heating up to 500 °C (10 °C/min) under He, in order to release/decompose the remaining N-species (previously adsorbed); since N-species balance during each NOx adsorption cycle pointed out a certain NOx adsorbed amount remaining at the end of the cycle.

The selectivity towards the different reduction products detected was estimated according to the following Equations (1)–(4). Even though very minor N_2O and NH_3 productions were monitored in some of the experiments, these compounds were also taken into account for calculation purposes:

$$S_{N_2}(\%) = 100 \cdot \frac{2n_{N_2}}{2n_{N_2} + n_{NO} + n_{NH_3} + 2n_{N_2O}}$$

$$S_{NO}(\%) = 100 \cdot \frac{n_{NO}}{2n_{N_2} + n_{NO} + n_{NH_3} + 2n_{N_2O}}$$

$$S_{NH_3}(\%) = 100 \cdot \frac{n_{NH_3}}{2n_{N_2} + n_{NO} + n_{NH_3} + 2n_{N_2O}}$$

$$S_{N_2O}(\%) = 100 \cdot \frac{2n_{N_2O}}{2n_{N_2} + n_{NO} + n_{NH_3} + 2n_{N_2O}}$$

where n_{N2}, n_{NO}, n_{N2O}, and n_{NH3} are the total molar amounts of N_2, NO, N_2O, and NH_3, respectively, evolved during the reduction phase and calculated by the integrals of the corresponding concentration curves vs. time.

Complementary in situ DRIFTS experiments were performed using a FT/IR-4000 Series spectrometer (JASCO Corporation, Tokyo, Japan), with a high-temperature reaction chamber, 4 cm^{-1} of resolution, and 16 scans per spectrum, in the 4000–500 cm^{-1} spectral range. The experiments were carried out in the interval of 150–350 °C, with approximately 60–70 mg of sample to fill the crucible, which was placed inside the reaction chamber; the flow was kept constant during the entire experiment, at 100 mL/min. Briefly, the sample was heated up to 500 °C under Ar and maintained for 30 min; after cooling down to the analysis temperature, the NO_x adsorption step was conducted by feeding 1000 ppm NO + 3% O_2 (*v*/*v*) in Ar to the reaction chamber for 1 h. After purging the chamber, the reduction step was carried out by feeding 2000 ppm H_2 in Ar for 1 h. A final TPD under Ar was conducted by heating the reaction chamber at 10 °C/min up to 500 °C. Every sequence of pre-treatment + NOx adsorption + H_2 reduction +TPD under He was conducted with a fresh sample. This specific procedure, along with the continuous presence of residual CO_2 in the pipes of the experimental set-up (even having a CO_2 absorber available), yielded to an experimental observation of persistent carbonate bands at all times on the catalysts' surfaces.

The complete analysis and discussion of the storage phase have been already deeply analyzed in a previous paper [48]. For this reason, the attention in this paper is focused on the reduction/decomposition step, reporting some data on the storage phase only to clarify purpose, if any.

3. Results and Discussion

3.1. NO_x Storage/Reduction Cycles.

Figure 1 shows a typical sequence of seven lean/rich cycles performed over the fully formulated Ba6/Cu2CZ catalyst at 300 °C. The concentration of all the gaseous species detected (i.e., NO, NO_2, NO_x, H_2, H_2O, N_2, NH_3, CO_2) are reported.

Upon NO and O_2 admission (at t = 0), NO concentration rapidly increases, while NO_2 formation is observed, with a slight delay due to the occurrence of NO oxidation by O_2, in line with previous results [48]. The NO_x adsorption process reasonably involves both Ba and Ce sites, even though NO_x adsorbed on Ba or on Ce sites is reported to be indistinguishable upon surface analysis. After NO admission, the evolution of H_2O is observed, accompanied in the first cycle by a small amount of CO_2. It is possible to correlate the latter to the barium carbonate decomposition during the NO_x adsorption, according to the global reaction:

$$BaCO_3 + 2\ NO + 3/2\ O_2 \rightarrow Ba(NO_3)_2 + CO_2 \quad (1)$$

After the first cycle, since CO_2 is absent in the gas stream and carbonates are not restored during the subsequent reduction step, the evolution of CO_2 is not observed anymore.

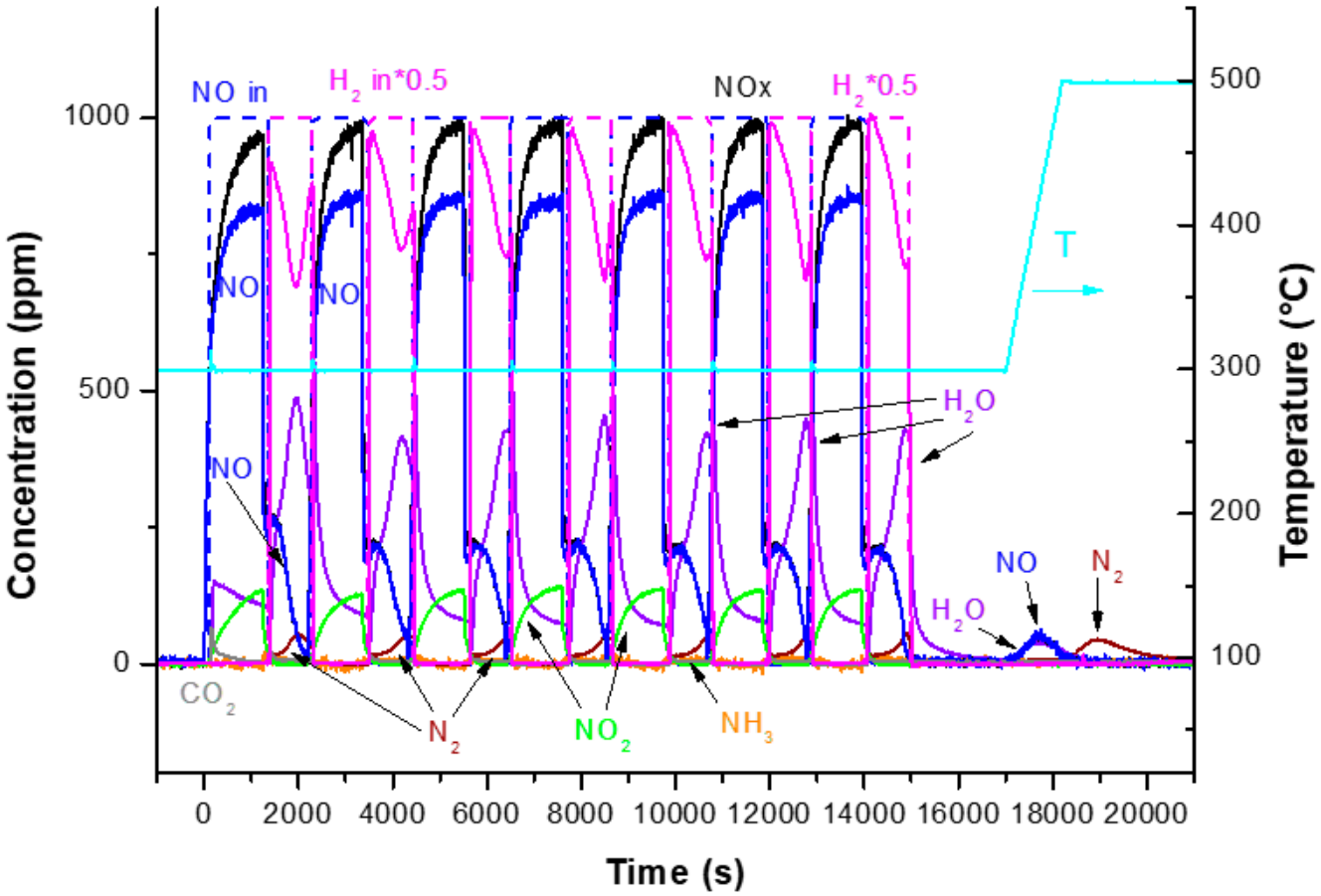

Figure 1. Profiles of product and inlet concentrations (in dashed lines) during NO_x storage and H_2 reduction consecutive pulses, carried out with Ba6/Cu2CZ at 300 °C.

On the other hand, H_2O desorption could be associated with the interaction between gas phase NO_x and the hydroxyl groups of the ceria-based catalysts, producing ad-NO_x surface species, as confirmed in a previous publication [48] and according to reactions (6) and (7):

$$NO + 2\ Ce^{4+} - OH^- \rightarrow Ce^{4+} - NO_2^- + Ce^{3+} - \square + H_2O \quad (2)$$

$$Ce^{4+} - NO_2^- + Ce^{4+} - O^* \rightarrow Ce^{4+} - NO_3^- + Ce^{3+} - \square \quad (3)$$

The outlet concentrations of both NO and NO_2 increase with time and eventually reach a steady-state level (with the exception of the first adsorption step). At the end of the adsorption phase, DRIFTS analysis reported in a previous work [48] (and on SI, as commented below) showed representative bands at 1245 and 1010 cm^{-1}, which were attributed to nitrate species stored on the catalyst surface (both on Ba and Ce sites) in different geometries and configurations.

At the end of every lean phase, the gas feed is switched to rich conditions to regenerate the catalyst surface from the stored NO_x. The H_2 concentration presents a relevant and complex profile; indeed, it increases with the simultaneous evolution of NO and H_2O, then decreases, reaching a minimum in correspondence with a maximum in the water evolution. N_2 and negligible amounts of NH_3 are monitored as N-reduction products. Accordingly, the ad-species stored on Ba sites (presumably nitrates) are reduced, following the global stoichiometry:

$$Ba(NO_3)_2 + H_2 \rightarrow NO/N_2/NH_3 + BaO + H_2O \quad (4)$$

Other reactions could take place concurrently during the rich phase:

$$BaO + H_2O \rightarrow Ba(OH)_2 \quad (5)$$

The latter could also partially explain the evolution of water during the new subsequent storage phase; indeed, when Ba hydroxides are involved in the storage, NO_x will scavenge H_2O and the evolution of this compound will occur. The reduction of NO_x stored over Ce sites are considered later on.

Quantitative analysis of the lean/rich cycle at 300 °C for Ba6/Cu2CZ is reported in Table 1 in terms of selectivity to reduction products (i.e., NO, N_2, NH_3) and N-balance evaluated as N-species adsorbed versus N-products evolved. As it appears, the catalyst exhibits almost the same behavior during all the cycles; indeed, the NO_x amounts stored is always near 250 μmol/g_{cat}, while the selectivity to N_2 is in the range of 26–34%. These results confirm the large stability of this catalyst during the seven cycles tested.

At the end of the lean-rich sequences, a desorption under the programmed temperature in inert atmosphere is carried out in order to completely remove the remaining superficial species. Indeed, as shown in Table 1, the N-balance results slightly higher than 1, suggesting that small amounts of NO_x remain adsorbed on the surface. As soon as the temperature increases, a release of NO is observed, with the maximum at 375 °C, followed by the subsequent emission of N_2, with the maximum at 500 °C. This is properly explained in the next section.

Table 1. Data from NO_x storage/H_2 reduction consecutive pulses (and final TPD), conducted at 300 °C for Ba6/Cu2CZ.

Cycle	NO_x Adsorbed (μmol/g_{cat})	Selectivity to N_2 (%)	Selectivity to NH_3 (%)	Selectivity to NO (%)	Balance [1] N_{ads}/N_{pr}
Cycle 1.	252	34	5	61	1.02
Cycle 2	255	31	3	66	1.02
Cycle 3	244	27	3	70	1.00
Cycle 4	246	28	3	69	1.01
Cycle 5	249	29	3	68	1.05
Cycle 6	252	27	3	70	1.02
Cycle 7	255	26	3	71	1.00

[1] Relationship between the NO_x adsorbed (during the NO_x pulse) and the released N-species in the reduction pulse.

3.2. Effect of Catalyst Formulation on the Reduction Phase

Lean/rich cycles at 150 °C and 300 °C are performed for the set of catalysts prepared (Figures 2a–d and 3a–e, respectively) to ascertain the influence of catalyst formulation. The mentioned Figures report H_2, H_2O, NO, NO_2, NH_3, N_2O, and N_2 outlet concentrations, along with the H_2 inlet profile (in dotted lines) of the rich phases corresponding to those cycles. The amounts of NO_x stored in the previous lean phase for every catalyst and adsorption temperature are compiled in Table S1 as Supplementary Data.

At 150 °C, the Cu-free CZ catalyst does not exhibit activity (Figure 2a). The activity of the other catalytic systems is very poor, whatever the composition of the catalyst. However, a small H_2 consumption can be observed with simultaneous H_2O production and NO generation (Figure 2b–d); indeed, very small amounts of NO_x were adsorbed onto the catalyst surface, thus being released in this rich step with the evolution of NO and water according to reaction (8), as already discussed. If Ba is not present in the catalyst formulation (Figure 2b), the cerium sites are the only sites responsible for NO_x adsorption (see Equations (6) and (7)); however, the evolution profile during the reduction step (NO and H_2O emission) seems to be qualitatively similar.

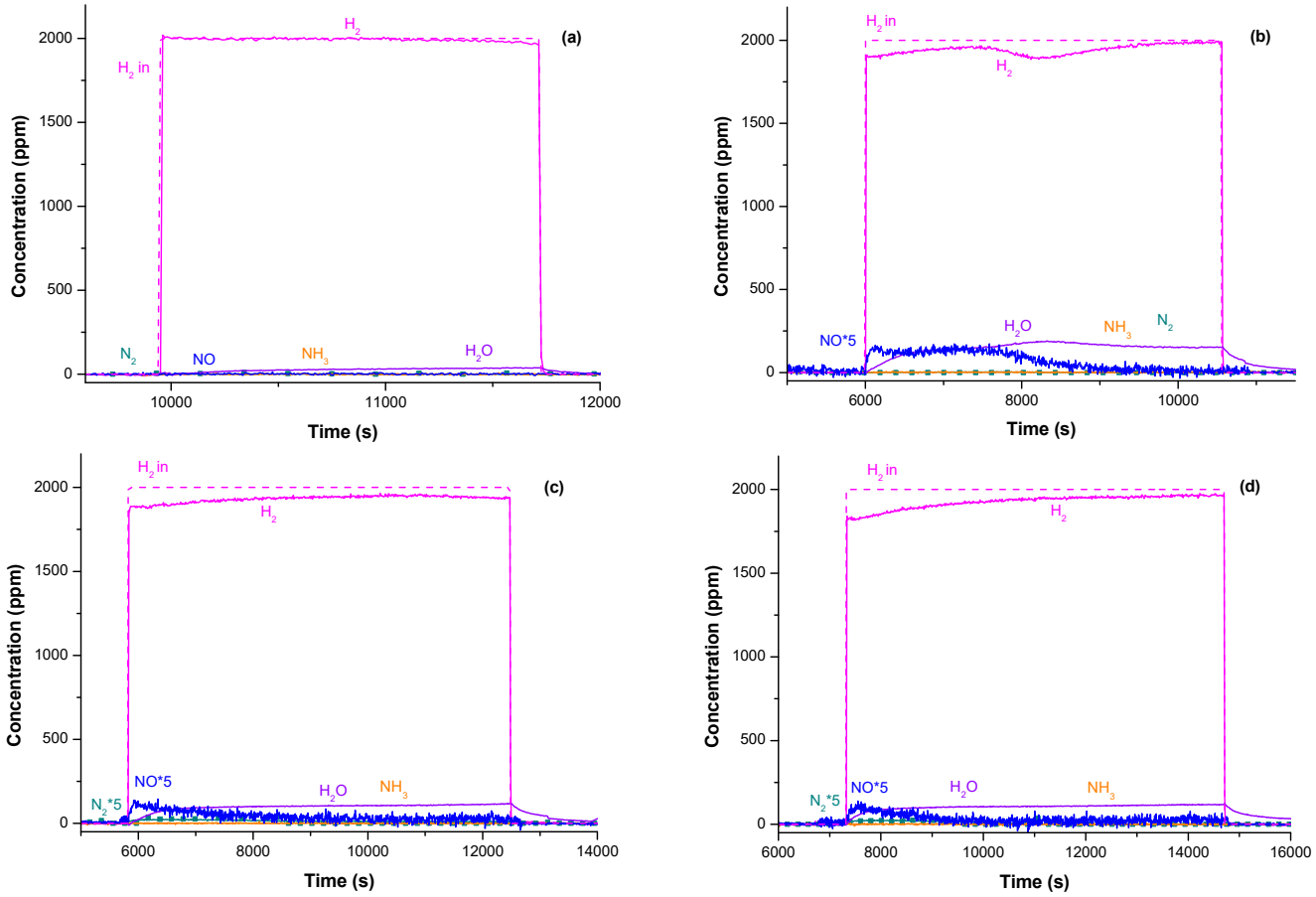

Figure 2. H_2, N_2, NH_3, NO, NO_2, and H_2O outlet concentrations, and H_2 inlet profile (in dotted lines) of the reduction step under 2000 ppm H_2, at 150 °C, for the catalysts: (**a**) CZ; (**b**) Cu2/CZ; (**c**) Ba6/Cu2CZ; and (**d**) Ba11/Cu2CZ (Ba6/CZ not included due to very low catalytic response).

The activity of the Cu-free catalysts (i.e., CZ and Ba6/CZ) at 300 °C is also low (Figure 3a,c); indeed, small H_2 consumptions were registered in line with the low reducibility of these samples. As a matter of fact, dedicated H_2-TPR experiments reported elsewhere [51] showed that the reduction did not take place in a reasonable extent until 400–500 °C. Moreover, a very small release of H_2O is observed, which is mostly ascribed to a small partial reduction of these catalysts with a small generation of oxygen vacancies [51]. Only negligible amounts of NO and NO_2 were detected for CZ, and there is no evidence of other N-containing products. It is suggested that the stored species are mainly decomposed to NO and/or NO_2, while they remain indifferent to the presence of H_2; this means that in the absence of Cu, H_2 is not activated and the catalysts do not reach an effective degree of reduction, which promotes the NO_x reduction process. On the other hand, in the case of Ba6/CZ (Figure 3c), no significant release of reduction or decomposition products is observed, indicating greater stability of ad-NO_x species with respect to bare CZ.

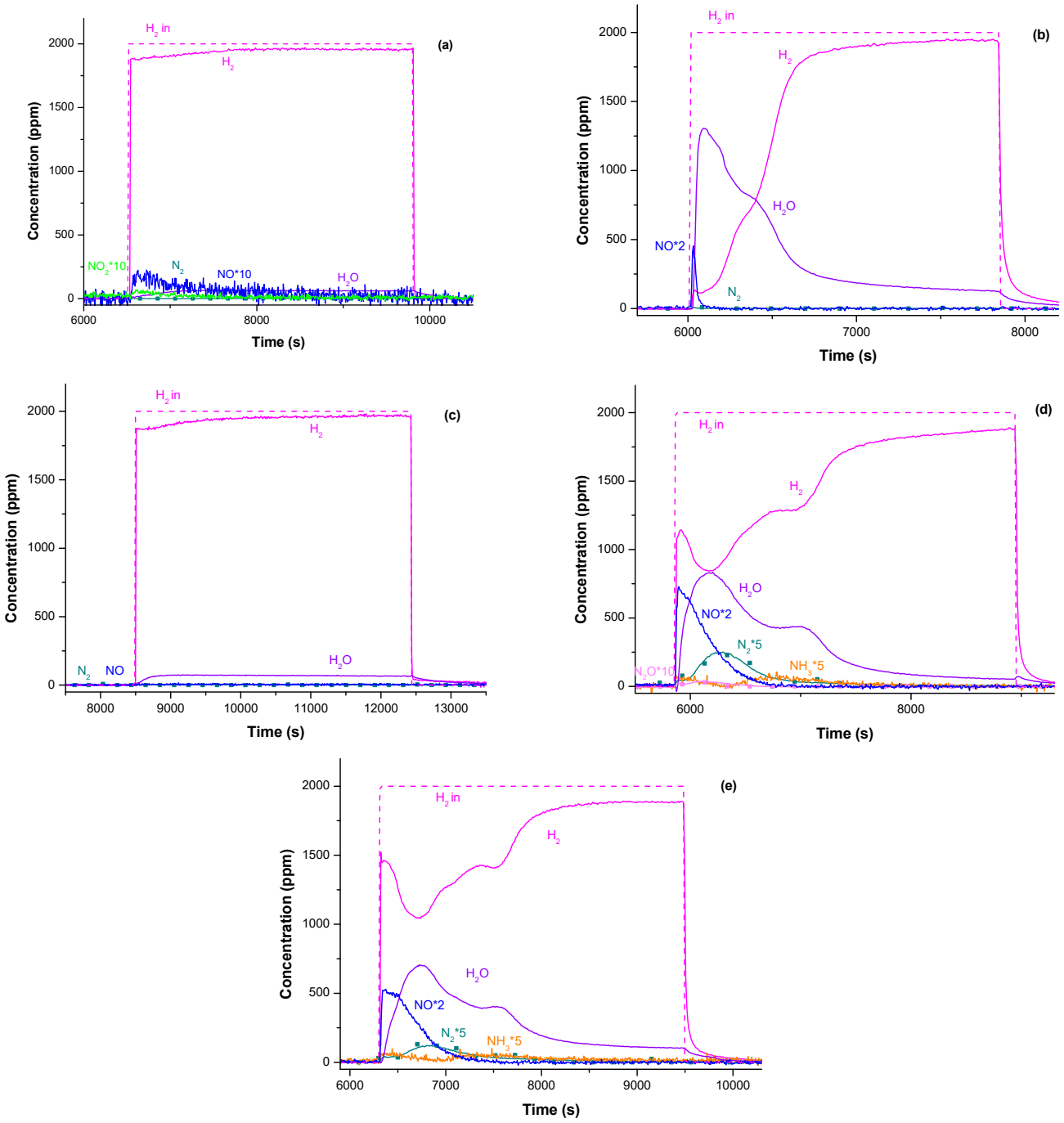

Figure 3. H_2, N_2, NH_3, NO, NO_2, and H_2O outlet concentrations, and H_2 inlet profile (in dotted lines) of the reduction step under 2000 ppm H_2, at 300 °C, for the catalysts: (**a**) CZ; (**b**) Cu2/CZ; (**c**) Ba6/CZ; (**d**) Ba6/Cu2CZ; and (**e**) Ba11/Cu2CZ.

Different features are observed when Cu is present in the catalyst formulation (i.e., in the case of the Cu2CZ and BaX/Cu2CZ catalysts, X = 6, 11 wt %). Indeed, in these cases (Figure 3b–e), a huge amount of water is produced upon H_2 admission, which generates a high population of oxygen vacancies, in line with the extension of the reduction of these catalysts in the range of 150–300 °C, as observed during the H_2-TPR experiments [48]. Considering the Cu2/CZ catalyst (Figure 3b), as soon as H_2 is admitted to the reactor, a very small and fast NO release is observed; the N-balance reveals that the very low amount of adsorbed NO_x (8.9 μmol/g_{cat}) is completely removed from the surface (see Table S1). The NO_x reduction is not selective to nitrogen, and only NO is detected during the

first minutes of the reduction phase. It is suggested that the NO produced during the reduction step is the result of the stored NO_x reduction and not of a decomposition, as observed in the case of Cu-free catalysts, since huge amounts of water are simultaneously produced that indicate the occurrence of such reduction.

Finally, by considering the fully formulated catalysts, i.e., Ba6/Cu2CZ and Ba11/Cu2CZ (Figure 3d,e) upon H_2 admission, NO is immediately observed, as in the previous case; however, after a very short period of time and in correspondence with the drop in NO concentration, N_2 evolves as well (together with very minor amounts of N_2O). NH_3 concentration deviates slightly from zero, although rigorous quantification is somewhat difficult. Huge amounts of H_2O are observed in both cases with a complex profile. The N-balance calculated in these cases is close to 1.

An analysis of the previous results suggests a close analogy with traditional NSR systems. Indeed, for BaX/Cu2CZ catalysts, NO_x is stored during the lean phase, forming nitrite and nitrate species as with the traditional Pt-Ba/Al_2O_3 NSR catalyst; the stored species are then reduced during the subsequent rich phase. However, the selectivity towards N_2 of the Ba-Cu catalyst is definitely lower, with NO being the main product; on the other hand, the decrease in the N_2 selectivity of Pt-based catalysts is related to the production of NH_3 and this drawback should be overcome by exploiting it in a SCR downstream catalytic bed.

The complex H_2 concentration profile and the delay in the N_2 emission suggests that before the catalyst becomes active in the stored NO_x reduction (i.e., before the production of N_2) some degree of reduction of the catalyst is required (i.e., a consumption of H_2 is observed at the beginning of the reduction phase without the creation of N-reduced products). Indeed, at the beginning of the reduction phase, its partial consumption after H_2 admission is observed together with H_2O production (Figure 3d,e); this could be explained by a catalyst reduction, which generates oxygen vacancies. In the meantime, the stored NO_x, present on the catalyst surface as nitrites/nitrates [51], are partially reduced to NO that is observed in the gas phase together with H_2 admission; indeed, as already observed, the catalyst is not sufficiently reduced to transform nitrites/nitrates into N_2, therefore only NO is produced. After a certain induction time, the catalyst reaches a sufficient reduction state and the released NO interacts with the oxygen vacancies being reduced to N_2, which is observed with a delay from the H_2 admission. Daturi et al. [52] explained the N_2 formation by the adsorption of two molecules of NO onto oxygen vacancies in close vicinity, and that their interaction yielded gaseous N_2 and the oxygen vacancies were filled with oxygen. On the other hand, Mihaylov et al. [53] described this N_2 formation with the generation of the hyponitrite species on an oxygen vacancy, by the adsorption of two NO molecules (reactions (10) and (11)); after that, they may decompose to N_2O (reaction (12)), which can react again with an oxygen vacancy and yield N_2 and re-fill the oxygen vacancy (reaction (13)). This last mechanism could explain the very small production of N_2O detected in Figure 3d. A tentative sequence of steps are presented below [54]:

$$-Ce^{3+} - \square - Ce^{3+} - + NO \rightarrow - Ce^{4+} - [NO]^{2-} - Ce^{4+} - \quad (6)$$

$$-Ce^{4+} - [NO]^{2-} - Ce^{4+} - + NO \rightarrow -Ce^{4+} - [N_2O_2]^{2-} - Ce^{4+} - \quad (7)$$

$$-Ce^{4+} - [N_2O_2]^{2-} - Ce^{4+} - \rightarrow -Ce^{4+} - O^{2-} - Ce^{4+} - + N_2O \quad (8)$$

$$-Ce^{3+} - \square - Ce^{3+} - + N_2O \rightarrow - Ce^{4+} - O^{2-} - Ce^{4+} - + N_2 \quad (9)$$

In order to provide consistent evidence that support the occurrence of such plausible mechanisms of NO_x reduction and pathways of formation for the N-reduction products exposed above, complementary NO reduction experiments are conducted with selected catalysts under simplified and controlled reaction conditions. The purpose of this fundamental study is to analyze how the NO molecules interact with the oxygen vacancies freshly created on the pre-reduced catalysts under H_2. The Supplementary Information

compiles the description of these catalytic tests. Briefly, Ba6/Cu2CZ is pre-reduced in H_2 at 350 °C, after which NO is admitted to the reactor at 50 °C or 250 °C; the corresponding profiles are reported in Figure 4 (Figure 4a,b, respectively). As can be seen, for the Ba6/Cu2CZ catalyst, after NO admission at 50 °C (Figure 4a), a huge production of N_2O and a lower amount of N_2 are observed, while the NO concentration curve increases slowly up to a steady state. The same behavior is observed after the NO reaction at a higher temperature (250 °C, Figure 4b) with faster kinetics in the reduction product formation.

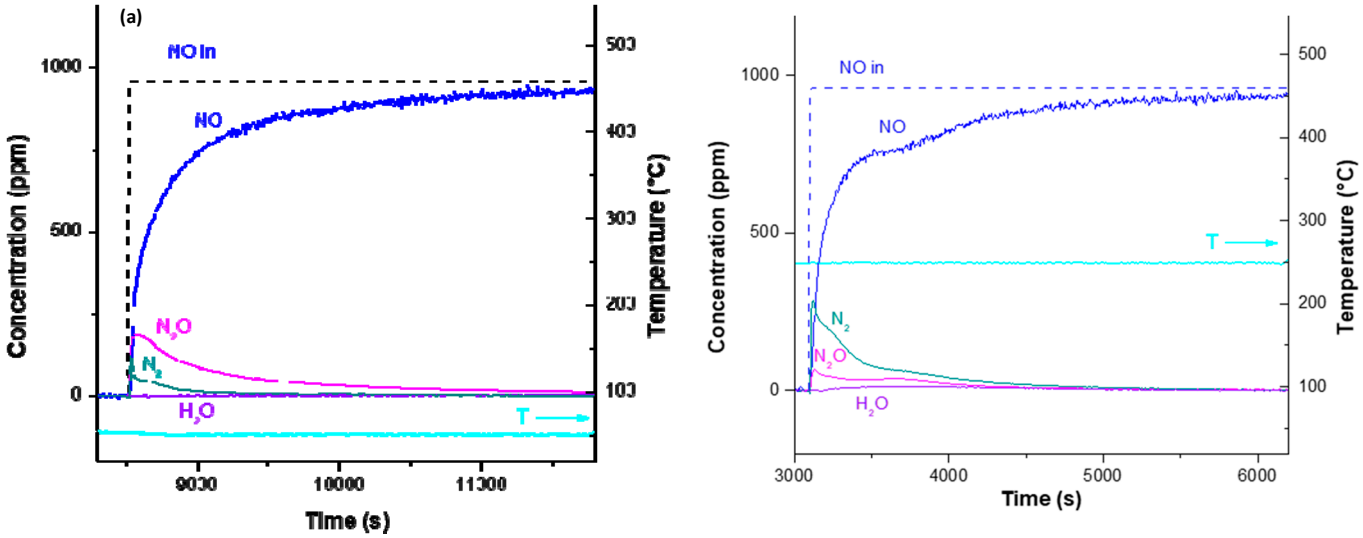

Figure 4. NO reduction experiment at 50 °C (**a**) and 250 °C (**b**) for pre-reduced Ba6/Cu2CZ.

Table 2 summarizes the quantitative analysis performed in the case of pre-reduced Ba6/Cu2CZ and Cu2/CZ catalysts as well. It clearly appears that the Ba-free catalyst is more reducible and higher amounts of N-products could be obtained with regard to Ba6/Cu2CZ. Likewise, it is noteworthy that selectivity towards N_2 depends on the NO reaction temperature, being higher at a higher temperature, according to the sequence of reactions (10)–(13).

According to these observations, it is proposed that during the pre-reduction in H_2, a population of oxygen vacancies is created; NO molecules subsequently interact with them, forming N-reduction products (see Table 2). It is worth noting that active sites linked to copper/ceria–zirconia's features are involved in the generation of oxygen vacancies. These, in turn, are able to reduce NO to N_2O and/or N_2; NH_3 is not observed under these experimental conditions. The order of product observation is in line with the proposed reaction scheme, i.e., N_2O before (reaction (12)), and eventually, N_2 (reaction (13)).

Table 2. Reaction data obtained during NO reduction reaction for pre-reduced Ba6/Cu2CZ and Cu2/CZ.

NO Reduction (50 or 250 °C)					
Catalyst [1]	**Temperature (°C)**	**NO Consumed (μmol/g_{cat})**	**N_2O Produced (μmol/g_{cat})**	**N_2 Produced (μmol/g_{cat})**	**N_2O/N_2 Ratio**
Ba6/Cu2CZ	50	511	186	34	5.5
Ba6/Cu2CZ	250	439	61	144	0.4
Cu2/CZ	50	784	315	72	4.4
Cu2/CZ	250	852	86	339	0.3

[1] Pre-reduction step under H_2 at 350 °C.

In summary, for the fully formulated catalysts where both Cu and Ba are present, a considerable amount of NO_x is stored onto the catalysts as nitrites/nitrates. Stored NO_x is then reduced to NO, which is in turn reduced to N_2O/N_2 (the latter being predominant) by its interaction with the oxygen vacancies; the selectivity to N_2 strictly depends on the degree of the catalyst reduction (i.e., Cu site reduction and the surrounding cerium centers), and therefore, on the population of oxygen vacancies that are created during the reduction step. Very minor NH_3 emissions detected in some experiments, (Figure 3d,e) could be explained by the occurrence of a global reaction (8), as previously anticipated.

In conclusion, it is clear that H_2 consumption during the rich phase (Figure 5) is related to both the reducibility of the catalyst and the reduction of the stored NO_x species. To estimate this consumption, the storage step is followed by a reduction of one hour under isothermal conditions. The quantitative analysis is reported in Figure 5 for the different catalysts and temperatures.

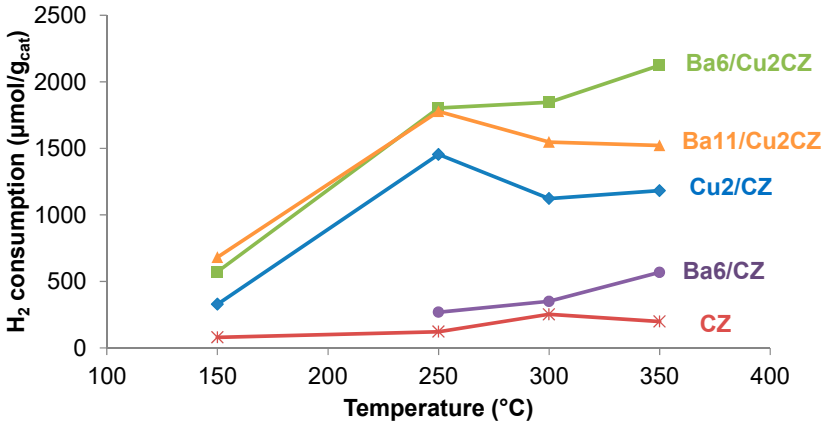

Figure 5. H_2 consumption in the reduction step (2000 ppm H_2 for 1 h) at several temperatures.

A very low reducibility is observed for bare CZ below 500 °C, as expected from the H_2-TPR results reported elsewhere [48]. On the contrary, the reducibility of Cu2/CZ is very high at low temperatures, starting from around 150 °C. This behavior agrees with the H_2 uptake estimated in the H_2 reduction phase (see Figure 5), where CZ consumes a very low amount of H_2, and Cu-containing catalysts present higher consumptions. In all cases, the evolution of water is observed along with H_2 consumption, thus indicating that some catalyst reduction is taking place. Most of H_2 consumption can be correlated to H_2O generation, but an accurate quantification of water is difficult and problematic in this case (as previously mentioned). In the H_2-TPR results presented elsewhere [48], additional evidence is provided of the catalyst reduction that occurs when the temperature of H_2 feeding is high enough. On the other hand, a part of these consumptions is attributed to nitrite/nitrate reduction and can be associated with the NO_x stored in the previous step, that being the copper-containing catalysts with higher consumptions. H_2 consumption does not increase linearly with temperature due to the creation of different populations of ad-NO_x species at different temperatures as a function of this variable.

A detailed inspection of Figure 5 reveals that there is a relative maximum of H_2 consumption at 250 °C in most of the samples. First of all, copper-containing samples achieve their maximum H_2 consumption at approximately 250 °C (in agreement with the H_2-TPR analyses), which should be accounted for in explaining the H_2 consumption trends observed. Therefore, a very low H_2 consumption is found at 150 °C; when the temperature is increased up to 250 °C or more, the catalysts are easily reduced. Cu-containing catalysts show different trends over 250 °C, which are directly related to the NO_x adsorption capac-

ity. Cu2/CZ shows a decrease in NO_x adsorption capacity together with temperature (congruent, with a corresponding decrease in H_2 consumption), while Ba/Cu-based catalysts present different trends when temperature goes up to 300 °C and 350 °C, respectively, with higher amounts of NO_x stored in the previous step. Ba11/Cu2CZ shows a lower H_2 consumption with respect to Ba6/Cu2CZ due to the slightly lower amount of Cu present when the Ba loading increases. On the other hand, copper-free samples show very low H_2 uptakes, becoming slightly higher when the temperature increases, which might be ascribed to the marginally enhanced reducibility of ceria–zirconia upon temperature increase, and also to the different nitrite/nitrate population creation on the Ba6/CZ and CZ with temperature. In summary, a balance between the NO_x adsorption capacity and the reduction extension, at whatever temperature, should be considered when analyzing H_2 consumption amounts in terms of temperature.

The evolution of surface species during the reduction phase was studied by in situ DRIFT analysis. Since the focus of this work is the reduction phase, the spectra recorded during the storage step, which represent the starting point of this analysis, are reported in Figures S3 and S4 in the Supplementary Information for the CZ and Ba6/CZ catalysts, respectively. Note that this characterization is possible for these two catalysts, while Cu is present, the dark-green color of the resultant samples leads to very low-intensity DRIFTS signals, making the DRIFT analysis very complex. However, with Ce and Ba as the adsorption sites, it is supposed that the spectra of the fully formulated Ba/Cu catalysts closely resemble those recorded for CZ and Ba6/CZ with respect to the nature of the adsorbed species, while Cu has more influence on the reduction dynamics. Figure 6a,b presents the DRIFTS spectra during the H_2 reduction step for CZ and Ba6/CZ, respectively, at 300 °C. For CZ, the band associated with adsorbed nitrate species (1279 cm^{-1}) [54,55], decreases in intensity during the reduction and completely disappears after 20 min; the same behavior is observed for the associate band at around 1025 cm^{-1}. In the region between 1600 and 1200 cm^{-1}, residual broad bands probably related to residual carbonates (e.g., 1482 cm^{-1}) are observed up to the end of the reduction phase. Regarding the adsorbed hydroxyl species, small changes can be observed during the reduction, although a slight increase in the band at 3637 cm^{-1} could be observed, since the desorption of water during this step could make the OH groups visible. Consistent with the absence of ad-NO_x species emission during the reduction step for Ba6/CZ, the corresponding spectra vary slightly along the course of the experiment, as depicted on Figure 6b, pointing out a great stability for the nitrites/nitrates generated on this catalyst, as anticipated above.

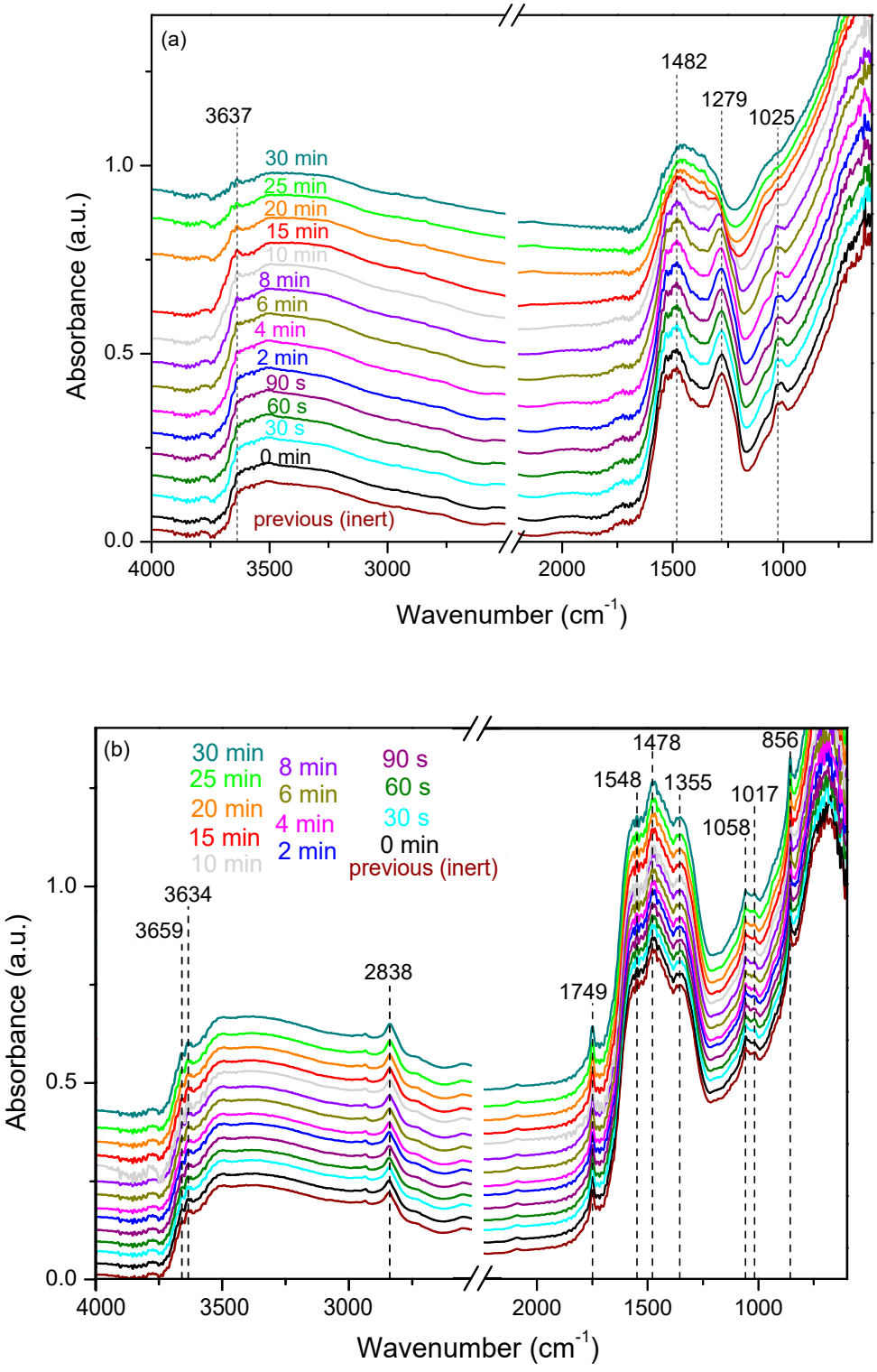

Figure 6. In situ DRIFTS spectra of CZ (**a**) and Ba6/CZ (**b**) during the reduction step in H_2, at 300 °C.

3.3. Thermal Desorption of Stored NO_x

In order to check the complete removal of stored NO_x from the surface after the reduction step, i.e., to verify the effectiveness of the H_2 reduction under these experimental conditions, a thermal decomposition was performed, heating every catalyst up to 500 °C in inert atmosphere. The corresponding concentration profiles are reported in Figures 7a–

d and 8a–e, referring to results after adsorption-reduction cycles at 150 °C and 300 °C, respectively.

In the case of the Cu-free sample (CZ) (Figure 7a), the decomposition of NO_x stored at 150 °C mainly yields the evolution of NO and O_2, and minor amounts of NO_2, in line with results reported in a previous work [54]. For this catalyst, NO is seen desorbed in two peaks, a small one at a low temperature (max near 230 °C) and a larger one at a high temperature (close to 415 °C, see Table 3).

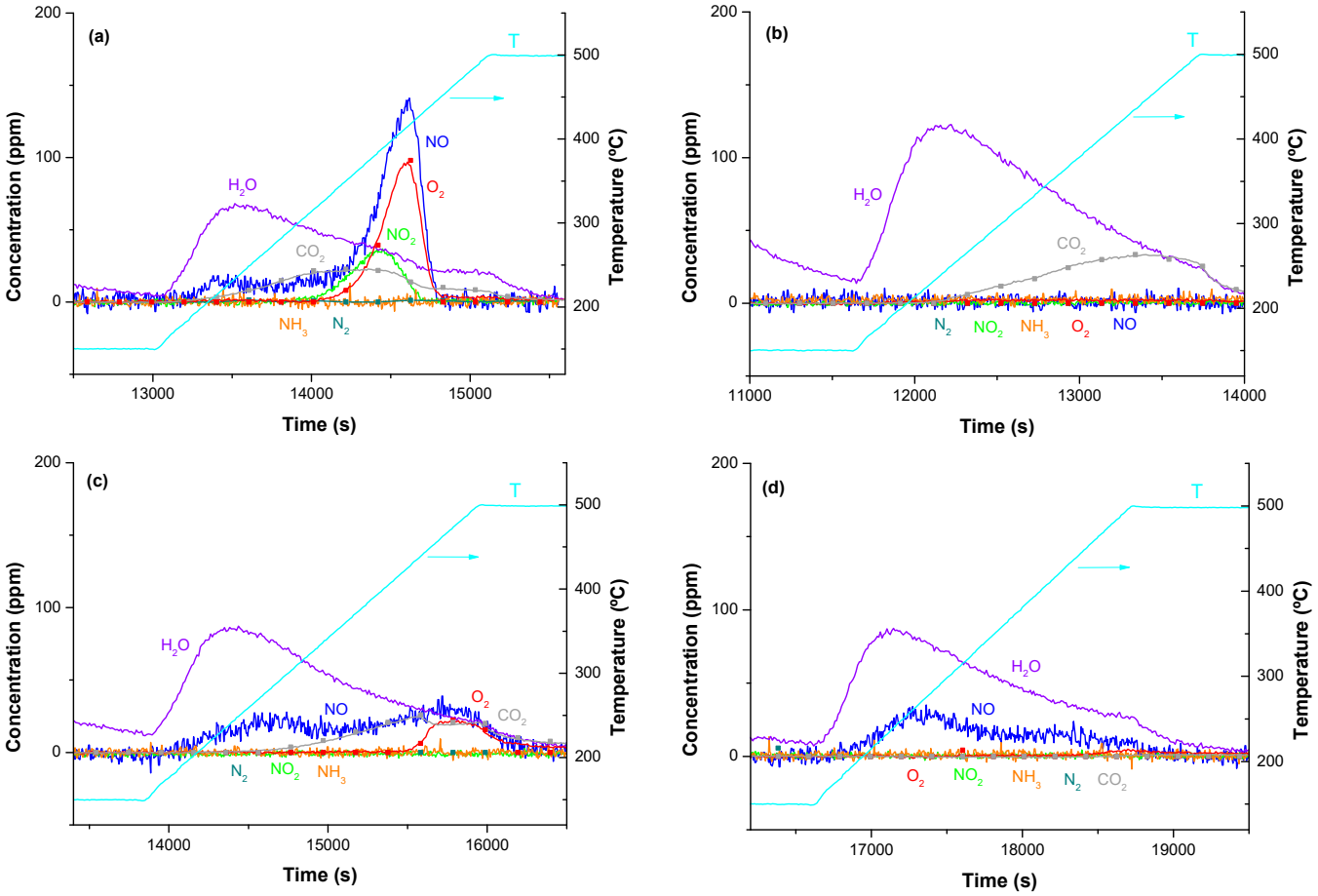

Figure 7. N_2, NH_3, NO, NO_2, O_2, and H_2O outlet concentrations during final TPD step, under He (after NO_x storage and H_2 reduction at 150 °C), for the catalysts: (**a**) CZ; (**b**) Cu2/CZ; (**c**) Ba6/Cu2CZ; and (**d**) Ba11/Cu2CZ. (Ba6/CZ not included due to very low catalytic response).

Table 3. NO_x/O_2 ratios estimated from the TPD step under He, for CZ and Ba6/CZ, after NO_x storage and reduction at the temperatures selected, and the corresponding temperature (T_{max}) of the maximum NO + O_2 release, in parenthesis.

Cycling Temperature	NO_x/O_2 Ratio and T_{max} (°C)	
	CZ	Ba6/CZ
150 °C	2.8 (415)	--
250 °C	2.8 (427)	1.4 (444)
300 °C	1.6 (426)	1.4 (445)
350 °C	1.6 (419)	1.3 (456)

For the rest of catalysts, different behaviors can be seen. For Cu2/CZ, all the ad-NO_x species stored are cleaned during the H_2 step. In the case of Ba11/Cu2CZ, only minor amounts of NO are desorbed. Ba6/Cu2CZ is characterized by an intermediate behavior.

NO_2 evolution is not detected, but at the highest temperatures (~450 °C, a double concomitant contribution NO/O_2 appears, similar to CZ). Since these peaks are shifted to higher temperatures (compared with those of CZ), this suggests that a lower amount of NO_x remains on the catalyst surface at the end of the cycling process, and that these species are more stable [19,34,56]; therefore, higher temperatures are required for these ad-NO_x species to suffer complete decomposition.

When the TPD is performed after cycling at 300 °C, the decomposition of the remaining stored NO_x produces only one temperature interval of desorption. For the NO_2 peak (the smallest one) and the NO/O_2 peaks, both in the case of CZ (Figure 8a) and Ba6/CZ (Figure 8c), the maximum is observed at 426 °C and 445 °C, respectively. This is in agreement with the idea explained above that the ad-NO_x species related to barium sites are more stable.

In order to establish if these decompositions can be attributed to nitrite and/or nitrate adsorbed species, the NO_x/O_2 molar ratio is calculated both from the experimental TPD profile and according to the stoichiometry of barium nitrites (reaction 14) and nitrates decomposition (reactions (15) and (16)):

$$Ba(NO_2)_2 \rightarrow BaO + 2NO + \tfrac{1}{2}O_2 \quad (10)$$

$$Ba(NO_3)_2 \rightarrow BaO + 2NO + \tfrac{3}{2}O_2 \quad (11)$$

$$Ba(NO_3)_2 \rightarrow BaO + 2NO_2 + \tfrac{1}{2}O_2 \quad (12)$$

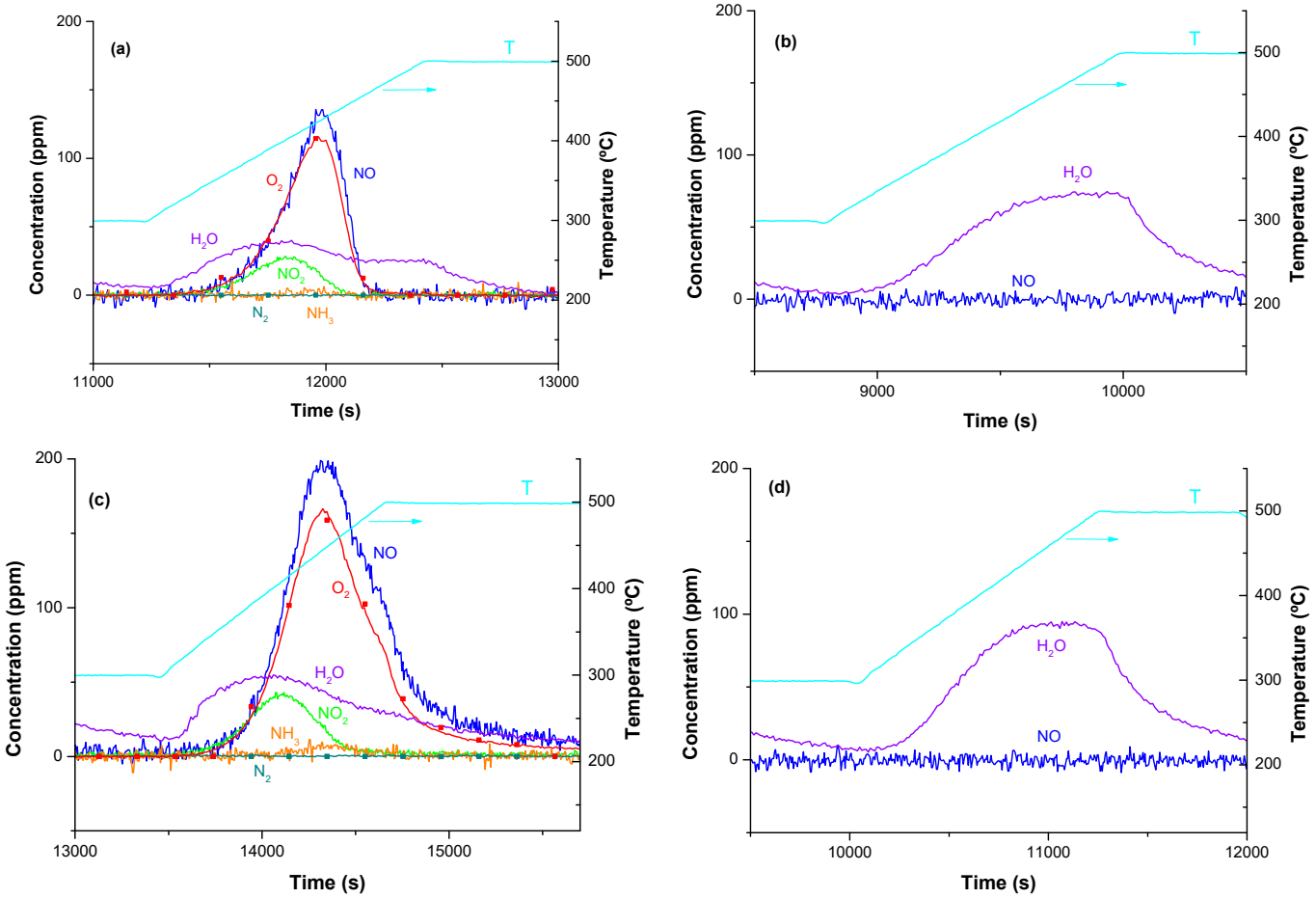

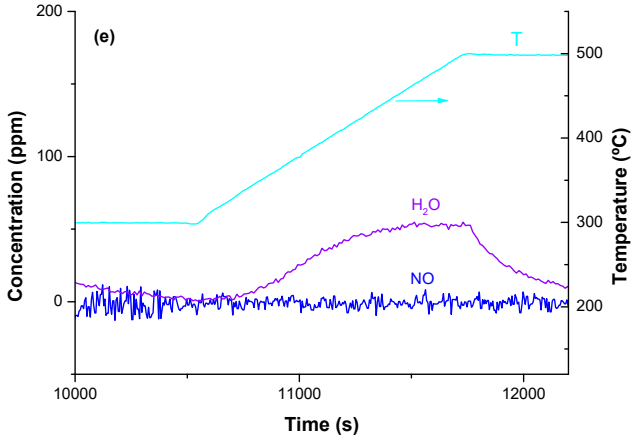

Figure 8. N_2, NH_3, NO, NO_2, O_2 and H_2O outlet concentrations during final TPD step, under He (after NO_x storage and H_2 reduction at 300 °C), for the catalysts: (**a**) CZ; (**b**) Cu2/CZ; (**c**) Ba6/CZ; (**d**) Ba6/Cu2CZ; and (**e**) Ba11/Cu2CZ.

The experimental NO_x/O_2 molar ratios for CZ and Ba6/CZ are collected in Table 3. As can be observed, in the case of CZ, the experimental NO_x/O_2 molar ratio is 2.8 at low temperature, suggesting a coexistence of mostly nitrites and nitrates on the catalyst surface, in accordance with the literature for ceria-based catalysts at low temperatures [19,54]. On the other hand, at high temperatures, a value near 1.3 is calculated, in line with the presence of nitrates (as verified by in situ DRIFTS experiments, Figure S3 on SI) adsorbed on this catalyst. On the contrary, Ba6/CZ presents values very close to 1.3, from 250 °C, which is theoretically attributed to barium nitrate decomposition [19], if it is assumed that most part of stored NO_x species are located on the Ba sites (reactions (14)–(16)). Therefore, it seems reasonable to establish that the NO_x species are stored mostly as nitrates in Ba6/CZ. Unfortunately, the corresponding in situ DRIFT spectra did not allow us to confirm this hypothesis (see Figure S4 in SI).

Considering the Cu-based catalyst, the resulting TPD profiles recorded after cycling at 150 °C (Figure 7b–d) and 300 °C (Figure 8b–e) are almost flat, i.e., without prominent peaks of NO_x species evolution. In the case of the Cu2/CZ system, this could be explained by the very low storage capacity of this system that results in the absence of NO_x on the catalyst surface at the end of the cycling process. On the other hand, in the case of Ba6/Cu2CZ and Ba11/Cu2CZ, this confirms the important role of copper in achieving the complete reduction of adsorbed NO_x species during cycling, which is an important feature that has to be accomplished when considering the design of effective NSR systems in combination with other after-treatment strategies.

4. Conclusions

This research was dedicated to the study of new PGM-free catalysts for the NO_x removal during LNT operation under simulated conditions. For this purpose, Ba-Cu/ceria–zirconia catalysts were synthetized, characterized, and tested by means of lean/rich cycles under isothermal conditions, at low temperatures, with particular attention to the reduction step in order to investigate their catalytic behavior in terms of the influence of copper presence on the catalytic formulations and the incorporation of different barium loadings to the ceria–zirconia support.

For Cu-free samples (i.e., CZ and Ba6/CZ) the addition of H_2 has the sole effect of partially reducing the catalytic surface, while the small amounts of stored NO_x are thermally decomposed to NO_2 and/or to NO/O_2 during the final TPD. On the other hand, for Cu-containing catalysts, N-products are detected during the rich phase, i.e., NO, N_2 with negligible amounts of NH_3, and N_2O. A mechanism for the stored NO_x reduction has been proposed, which involves the formation of oxygen vacancies over the Ce sites responsible for the reduction of released NO_x to N_2 and N_2O.

These results are promising since they give us the idea that Cu/ceria-based catalysts can produce N_2 even in the absence of noble metals. Further investigations on this aspect can be carried out in the future, focusing on the optimization of ceria-based materials for efficient NO_x storage and reduction processes and yielding N_2 as the main product, since very few investigations have been published in this area using these kinds of materials and obtaining such detailed information in terms of the nature of evolved products, the selectivity towards the desired products, and mass balances, as far as the authors are concerned.

However, it is worth considering that other different reaction pathways might occur, involving the generation of nitrites and nitrates on the catalysts' surfaces. In fact, other related reactions' mechanisms have been published in the literature to explain the NO_x interactions with cerium sites and oxygen vacancies, yielding the formation of mostly nitrites, hyponitrites, and nitrates.

Supplementary Materials: The following are available online at www.mdpi.com/article/10.3390/app11125700/s1.

Author Contributions: Conceptualization, L.C. and A.G.-G.; methodology, J.C.M.-M., J.G.-M., R.M., L.C. and A.G.-G.; validation, L.C. and A.G.-G.; formal analysis, J.C.M.-M. and J.G.-M.; investigation, J.C.M.-M and, J.G.-M.; data curation, J.C.M.-M., J.G.-M., and R.M.; writing—original draft preparation, J.G.-M., L.C. and A.G.-G.; writing—review and editing, J.C.M.-M., R.M., L.C. and A.G.-G.; supervision, A.G.-G.; funding acquisition, A.G.-G. All authors have read and agreed to the published version of the manuscript.

Funding: This research was funded by the financial support from the Generalitat Valenciana (PROMETEO/2018/076 project) and the Spanish Ministry of Science and Innovation (PID2019-105542RB-I00 project) and the UE-FEDER funding. J.C.M.-M. also acknowledges Spanish Ministry of Science and Innovation for the financial support through an FPU grant (FPU17/00603).

Institutional Review Board Statement: Not applicable.

Informed Consent Statement: Not applicable.

Data Availability Statement: Data sharing not applicable.

Conflicts of Interest: The authors declare no conflict of interest.

References

1. European Parliament"Curbing CO_2 Emissions from Cars: Agreement with Council", European Parliament, Brussels, 2018, https://www.europarl.europa.eu/news/en/press-room/20181218IPR22101/curbing-co2-emissions-from-cars-agreement-with-council (accessed on 1 March 2021).
2. Joshi, A. Review of Vehicle Engine Efficiency and Emissions. *SAE Tech. Pap.* **2020**, *5*, 2479–2507, doi:10.4271/2020-01-0352.
3. European Automobile Manufacturers Association (ACEA). ACEA Views on Preparing to Consider a next EU Emissions Stage–General Principles. In *EU Commission Stakeholder Event*; European Automobile Manufacturers Association (ACEA): Brussels, Belgium, 2018.
4. Mork, A.; Heimermann, C.; Schüttenhelm, M.; Frambourg, M. CO_2-Lighthouse Diesel Engine from Volkswagen Group Research. In Proceedings of the 27th Aachen Colloquium Automobile and Engine Technology, Aachen, Germany, 2018.
5. Schaub, J.; Kotter, M.; and Korfer, T. 48 V MHEV Diesel-Balancing Fuel Economy and Performance While Keeping Emission Advantages. In Proceedings of the FEV Diesel Powertrains 3.0 Conference, Coventry, UK, 2018.
6. Twigg, M.V. Catalytic control of emissions from cars. *Catal. Today* **2011**, *163*, 33–41, doi:10.1016/j.cattod.2010.12.044.
7. Gandhi, H.; Graham, G.; McCabe, R. Automotive exhaust catalysis. *J. Catal.* **2003**, *216*, 433–442, doi:10.1016/s0021-9517(02)00067-2.
8. Roy, S.; Hegde, M.; Madras, G. Catalysis for NOx abatement. *Appl. Energy* **2009**, *86*, 2283–2297, doi:10.1016/j.apenergy.2009.03.022.
9. Ayo, B.P.; De La Torre, U.; Illán-Gómez, M.J.; Bueno-López, A.; González-Velasco, J.R. Role of the different copper species on the activity of Cu/zeolite catalysts for SCR of NOx with NH_3. *Appl. Catal. B: Environ.* **2014**, *147*, 420–428, doi:10.1016/j.apcatb.2013.09.010.
10. Lietti, L.; Forzatti, P.; Nova, I.; Tronconi, E. NOx Storage Reduction over Pt Ba/γ-Al_2O_3 Catalyst. *J. Catal.* **2001**, *204*, 175–191, doi:10.1006/jcat.2001.3370.
11. Epling, W.S.; Campbell, L.E.; Yezerets, A.; Currier, N.W.; Parks, J.E. Overview of the Fundamental Reactions and Degradation Mechanisms of NOx Storage/Reduction Catalysts. *Catal. Rev.* **2004**, *46*, 163–245, doi:10.1081/cr-200031932.

12. Granger, P.; Parvulescu, V.I. Catalytic NOxAbatement Systems for Mobile Sources: From Three-Way to Lean Burn after-Treatment Technologies. *Chem. Rev.* **2011**, *111*, 3155–3207, doi:10.1021/cr100168g.
13. Forzatti, P.; Lietti, L.; Castoldi, L. Storage and Reduction of NO x Over LNT Catalysts. *Catal. Lett.* **2015**, *145*, 483–504, doi:10.1007/s10562-014-1343-0.
14. Say, Z.; Vovk, E.I.; Bukhtiyarov, V.I.; Ozensoy, E. Influence of ceria on the NOx reduction performance of NOx storage reduction catalysts. *Appl. Catal. B Environ.* **2013**, *142–143*, 89–100, doi:10.1016/j.apcatb.2013.04.075.
15. Roy, S.; Baiker, A. NOx Storage−Reduction Catalysis: From Mechanism and Materials Properties to Storage−Reduction Performance. *Chem. Rev.* **2009**, *109*, 4054–4091, doi:10.1021/cr800496f.
16. Nova, I.; Castoldi, L.; Lietti, L.; Tronconi, E.; Forzatti, P.; Prinetto, F.; Ghiotti, G. NOx adsorption study over Pt–Ba/alumina catalysts: FT-IR and pulse experiments. *J. Catal.* **2004**, *222*, 377–388, doi:10.1016/j.jcat.2003.11.013.
17. Kubiak, L.; Castoldi, L.; Lietti, L.; Andonova, S.; Olsson, L. Mechanistic Investigation of the Reduction of NOx over Pt- and Rh-Based LNT Catalysts. *Catalysts* **2016**, *6*, 46, doi:10.3390/catal6030046.
18. Castoldi, L.; Righini, L.; Matarrese, R.; Lietti, L.; Forzatti, P. Mechanistic aspects of the release and the reduction of NO stored on Pt–Ba/Al_2O_3. *J. Catal.* **2015**, *328*, 270–279, doi:10.1016/j.jcat.2015.02.005.
19. Infantes-Molina, A.; Righini, L.; Castoldi, L.; Loricera, C.; Fierro, J.; Sin, A.; Lietti, L. Characterization and reactivity of Ce-promoted PtBa lean NOx trap catalysts. *Catal. Today* **2012**, *197*, 178–189, doi:10.1016/j.cattod.2012.07.036.
20. Stanmore, B.; Brilhac, J.; Gilot, P. The oxidation of soot: A review of experiments, mechanisms and models. *Carbon* **2001**, *39*, 2247–2268, doi:10.1016/s0008-6223(01)00109-9.
21. Jeguirim, M.; Tschamber, V.; Brilhac, J.F. Kinetics of catalyzed and non-catalyzed soot oxidation with nitrogen dioxide under regeneration particle trap conditions. *J. Chem. Technol. Biotechnol.* **2009**, *84*, 770–776, doi:10.1002/jctb.2110.
22. Jeguirim, M.; Tschamber, V.; Ehrburger, P. Catalytic effect of platinum on the kinetics of carbon oxidation by NO_2 and O_2. *Appl. Catal. B Environ.* **2007**, *76*, 235–240, doi:10.1016/j.apcatb.2007.05.029.
23. Jacquot, F.; Logie, V.; Brilhac, J.F.; Gilot, P. Kinetics of the Oxidation of Carbon Black by NO_2 Influence of the Presence of Water and Oxygen. *Carbon* **2002**, *40*, 335–343.
24. Castoldi, L.; Artioli, N.; Matarrese, R.; Lietti, L.; Forzatti, P. Study of DPNR catalysts for combined soot oxidation and NOx reduction. *Catal. Today* **2010**, *157*, 384–389, doi:10.1016/j.cattod.2010.03.022.
25. Castoldi, L.; Matarrese, R.; Lietti, L.; Forzatti, P. Simultaneous removal of NOx and soot on Pt–Ba/Al_2O_3 NSR catalysts. *Appl. Catal. B Environ.* **2006**, *64*, 25–34, doi:10.1016/j.apcatb.2005.10.015.
26. Fino, D.; Specchia, V. Open issues in oxidative catalysis for diesel particulate abatement. *Powder Technol.* **2008**, *180*, 64–73, doi:10.1016/j.powtec.2007.03.021.
27. Suzuki, J.; Matsumoto, S. Development of Catalysts for Diesel Particulate NOx Reduction. *Top. Catal.* **2004**, *28*, 171–176, doi:10.1023/b:toca.0000024347.67237.f6.
28. Ren, Y.Y.; Deng, C.S.; Ai, D.S.; Ma, J.T.; Zan, Q.F.; Kong, J.R.; Xu, J.M. A Facile Template-Free Synthesis of Praseodym-ium-Doped Ceria Nanorods. *Key Eng. Mater.* **2010**, *434–435*, 714–716.
29. Rovira, L.G.; Delgado, J.J.; Elamrani, K.; Del Rio, E.; Chen, X.; Calvino, J.J.; Botana, F.J. Synthesis of ceria-praseodimia nanotubes with high catalytic activity for CO oxidation. *Catal. Today* **2012**, *180*, 167–173, doi:10.1016/j.cattod.2011.05.006.
30. Liang, Q.; Wu, X.; Weng, D.; Xu, H. Oxygen activation on Cu/Mn–Ce mixed oxides and the role in diesel soot oxidation. *Catal. Today* **2008**, *139*, 113–118, doi:10.1016/j.cattod.2008.08.013.
31. Giménez-Mañogil, J.; Guillén-Hurtado, N.; Fernández-García, S.; Chen, X.; Calvino-Gámez, J.J.; García-García, A. Ceria-Praseodymia Mixed Oxides: Relationships Between Redox Properties and Catalytic Activities Towards NO Oxidation to NO_2 and CO-PROX Reactions. *Top. Catal.* **2016**, *59*, 1065–1070, doi:10.1007/s11244-016-0591-1.
32. López, A.B.; Lozano-Castelló, D.; Anderson, J.A. NOx storage and reduction over copper-based catalysts. Part 2: Ce 0.8 M 0.2 O δ supports (M = Zr, La, Ce, Pr or Nd). *Appl. Catal. B Environ.* **2016**, *198*, 234–242, doi:10.1016/j.apcatb.2016.05.066.
33. Piacentini, M.; Maciejewski, M.; Baiker, A. Supported Pt-Ba NOx storage-reduction catalysts: Influence of support and Ba loading on stability and storage efficiency of Ba-containing species. *Appl. Catal. B Environ.* **2006**, *66*, 126–136, doi:10.1016/j.apcatb.2006.02.002.
34. Ji, Y.; Toops, T.J.; Crocker, M. Effect of Ceria on the Storage and Regeneration Behavior of a Model Lean NO x Trap Catalyst. *Catal. Lett.* **2007**, *119*, 257–264, doi:10.1007/s10562-007-9226-2.
35. Giménez-Mañogil, J.; García-García, A. Identifying the nature of the copper entities over ceria-based supports to promote diesel soot combustion: Synergistic effects. *Appl. Catal. A Gen.* **2017**, *542*, 226–239, doi:10.1016/j.apcata.2017.05.031.
36. Martinez-Arias, A.; Gamarra, D.; Fernández-García, M.; Hornés, A.; Bera, P.; Koppány, Z.; Schay, Z. Redox-catalytic correlations in oxidised copper-ceria CO-PROX catalysts. *Catal. Today* **2009**, *143*, 211–217, doi:10.1016/j.cattod.2008.09.018.
37. Marbán, G.; Fuertes, A.B. Highly active and selective CuOx/CeO_2 catalyst prepared by a single-step citrate method for preferential oxidation of carbon monoxide. *Appl. Catal. B Environ.* **2005**, *57*, 43–53, doi:10.1016/j.apcatb.2004.10.011.
38. Martínez-Arias, A.; Hungría, A.; Munuera, G.; Gamarra, D. Preferential oxidation of CO in rich H_2 over CuO/CeO_2: Details of selectivity and deactivation under the reactant stream. *Appl. Catal. B Environ.* **2006**, *65*, 207–216, doi:10.1016/j.apcatb.2006.02.003.
39. Jia, A.-P.; Jiang, S.-Y.; Lu, J.-Q.; Luo, M.-F. Study of Catalytic Activity at the CuO−CeO_2 Interface for CO Oxidation. *J. Phys. Chem. C* **2010**, *114*, 21605–21610, doi:10.1021/jp108556u.

40. Martínez-Arias, A.; Fernández-García, M.; Gálvez, O.; Coronado, J.M.; Anderson, J.A.; Conesa, J.C.; Soria, J.; Munuera, G. Comparative Study on Redox Properties and Catalytic Behavior for CO Oxidation of CuO/CeO_2 and CuO/$ZrCeO_4$ Catalysts. *J. Catal.* **2000**, *195*, 207–216, doi:10.1006/jcat.2000.2981.
41. Martínez-Arias, A.; Gamarra, D.; Fernández-García, M.; Wang, X.; Hanson, J.; Rodriguez, J. Comparative study on redox properties of nanosized CeO_2 and CuO/CeO_2 under CO/O_2. *J. Catal.* **2006**, *240*, 1–7, doi:10.1016/j.jcat.2006.02.026.
42. Jia, A.-P.; Hu, G.; Meng, L.; Xie, Y.-L.; Lu, J.-Q.; Luo, M.-F. CO oxidation over CuO/$Ce_{1-x}Cu_xO_{2-\delta}$ and $Ce_{1-x}Cu_xO_{2-\delta}$ catalysts: Synergetic effects and kinetic study. *J. Catal.* **2012**, *289*, 199–209, doi:10.1016/j.jcat.2012.02.010.
43. MartínezAriasA.; Fernández-García, M.; Soria, J.; Conesa, J. Spectroscopic Study of a Cu/CeO_2Catalyst Subjected to Redox Treatments in Carbon Monoxide and Oxygen. *J. Catal.* **1999**, *182*, 367–377, doi:10.1006/jcat.1998.2361.
44. Giménez-Mañogil, J.; Bueno-López, A.; García-García, A. Preparation, characterisation and testing of CuO/$Ce_{0.8}Zr_{0.2}O_2$ catalysts for NO oxidation to NO_2 and mild temperature diesel soot combustion. *Appl. Catal. B Environ.* **2014**, *152–153*, 99–107, doi:10.1016/j.apcatb.2014.01.018.
45. Giménez-Mañogil, J.; García-García, A. Opportunities for ceria-based mixed oxides versus commercial platinum-based catalysts in the soot combustion reaction. Mechanistic implications. *Fuel Process. Technol.* **2015**, *129*, 227–235, doi:10.1016/j.fuproc.2014.09.018.
46. Giménez-Mañogil, J.; Quiles-Díaz, S.; Guillén-Hurtado, N.; García-García, A. Catalyzed Particulate Filter Regeneration by Platinum Versus Noble Metal-Free Catalysts: From Principles to Real Application. *Top. Catal.* **2017**, *60*, 2–12, doi:10.1007/s11244-016-0730-8.
47. Quiles-Díaz, S.; Giménez-Mañogil, J.; García-García, A. Catalytic performance of CuO/$Ce_{0.8}Zr_{0.2}O_2$ loaded onto SiC-DPF in NO_x-assisted combustion of diesel soot. *RSC Adv.* **2015**, *5*, 17018–17029, doi:10.1039/C4RA15595E.
48. Giménez-Mañogil, J.; Martínez-Munuera, J.C.; Matarrese, R.; Castoldi, L.; Lietti, L.; García-García, A. NOx Adsorption Over Ce/Zr-Based Catalysts Doped with Cu and Ba. *Top. Catal.* **2019**, *62*, 140–149, doi:10.1007/s11244-018-1130-z.
49. Atribak, I.; López, A.B.; Garcia-Garcia, A. Combined removal of diesel soot particulates and NOx over CeO_2–ZrO_2 mixed oxides. *J. Catal.* **2008**, *259*, 123–132, doi:10.1016/j.jcat.2008.07.016.
50. Guillén-Hurtado, N.; Bueno-López, A.; García-García, A. Surface and structural characterisation of coprecipitated $Ce_xZr_{1-x}O_2$ ($0 \le x \le 1$) mixed oxides. *J. Mater. Sci.* **2011**, *47*, 3204–3213, doi:10.1007/s10853-011-6158-4.
51. Martínez-Munuera, J.; Giménez-Mañogil, J.; Castoldi, L.; Lietti, L.; García-García, A. Ceria-based catalysts for NO_x removal in NSR processes: A fundamental study of the catalyst modifications explored by in situ techniques. *Appl. Surf. Sci.* **2020**, *529*, 147019, doi:10.1016/j.apsusc.2020.147019.
52. Daturi, M.; Bion, N.; Saussey, J.; LaValley, J.-C.; Hedouin, C.; Séguelong, T.; Blanchard, G. Evidence of a lacunar mechanism for deNOx activity in ceria-based catalysts. *Phys. Chem. Chem. Phys.* **2000**, *3*, 252–255, doi:10.1039/b007818m.
53. Mihaylov, M.; Ivanova, E.Z.; Aleksandrov, H.; Petkov, P.S.; Vayssilov, G.N.; Hadjiivanov, K.I. FTIR and density functional study of NO interaction with reduced ceria: Identification of N_3^- and NO^{2-} as new intermediates in NO conversion. *Appl. Catal. B Environ.* **2015**, *176–177*, 107–119, doi:10.1016/j.apcatb.2015.03.054.
54. Atribak, I.; Azambre, B.; López, A.B.; García-García, A. Effect of NO_x adsorption/desorption over ceria-zirconia catalysts on the catalytic combustion of model soot. *Appl. Catal. B Environ.* **2009**, *92*, 126–137, doi:10.1016/j.apcatb.2009.07.015.
55. Azambre, B.; Zenboury, L.; Delacroix, F.; Weber, J. Adsorption of NO and NO_2 on ceria–zirconia of composition $Ce_{0.69}Zr_{0.31}O_2$: A DRIFTS study. *Catal. Today* **2008**, *137*, 278–282, doi:10.1016/j.cattod.2007.09.003.
56. Martínez-Arias, A.; Soria, J.; Conesa, J.C.; Seoane, X.L.; Arcoya, A.; Cataluña, R. NO reaction at surface oxygen vacancies generated in cerium oxide. *J. Chem. Soc. Faraday Trans.* **1995**, *91*, 1679–1687, doi:10.1039/ft9959101679.